Recombinant erythropoietin in urine

An artificial hormone taken to boost athletic performance can now be detected.

Erythropoietin is a hormone that stimulates the production of new red blood cells (erythropoiesis). Although athletes use recombinant human erythropoietin illicitly to boost the delivery of oxygen to the tissues and enhance their performance in endurance sports, this widespread doping practice cannot be controlled in the absence of a reliable analytical procedure to monitor it. Here we describe a new technique for detecting this drug in urine following its recent administration.

The stimulation of erythropoiesis by erythropoietin (EPO) makes this drug very attractive to sportspeople wishing to improve their aerobic power, although the International Olympic Committee banned its misuse ten years ago. Detection has been a problem — analysis of haematological[1] or biochemical[2] parameters indicates only that erythropoiesis has been stimulated, but cannot confirm that drug administration is to blame.

To detect administered hormone directly means that exogenous, recombinant EPO must be differentiated from natural, endogenous EPO. A promising electrophoretic method[3] has proved impractical for screening by the antidoping laboratories. We have developed an analytical procedure for detecting recombinant EPO in urine and have applied it to specimens from cyclists participating in the the infamous Tour de France 1998 competition, which was sullied by scandals about EPO doping.

Owing to microheterogeneity in their structures, natural and recombinant EPO comprise several isoforms, some of which have charge differences and can be separated by isoelectric focusing (Fig. 1). We found that the isoelectric patterns of the two recombinant EPO-α and -β forms are very similar (both have an isoelectric point, pI, in the range 4.42–5.11); although EPO-β has an extra basic band, both differ from natural, purified urinary EPO, which has more acidic bands (pI 3.92–4.42), probably due to post-translational modifications such as glycosylation, which is species- and tissue-type-dependent[4]. Such differences in the urine analysis allowed us to ascribe excreted EPO to a natural or recombinant origin.

We developed an immunoblotting procedure to obtain a reliable image of EPO patterns in urine. Our results (Fig. 1) indicated that the patterns from control subjects consisted of about 10 bands of pI 3.77–4.70, in accord with the purified natural urinary EPO pattern, whereas those from subjects treated with recombinant EPO contained more basic bands, reflecting the presence of recombinant isoforms, and sometimes acidic bands as well, depending on the presence of endogenous isoforms. The presence of exogenous hormone was always evident: any individual injected with recombinant EPO showed a striking transformation of their initial EPO urine pattern.

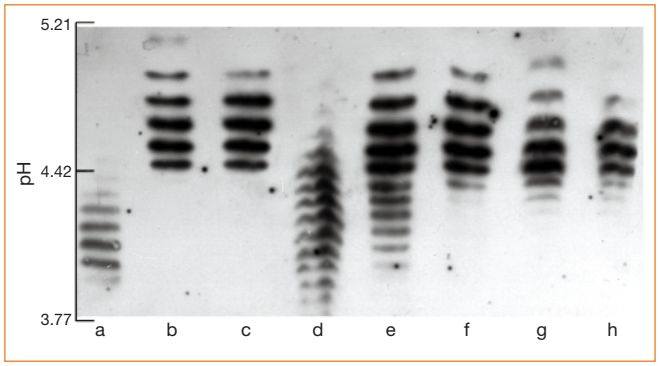

Figure 1 Autoradiograph of isoelectric patterns of exogenous and endogenous erythropoietin (EPO). Images were obtained by chemiluminescent immunodetection of blotted EPO after isoelectric focusing. **a,** Purified commercial human urinary natural EPO (Sigma); **b,** recombinant EPO-β (Neorecormon, France); **c,** recombinant EPO-α (Eprex, France); **d,** urine from a control subject; **e,f,** urine from two patients treated with Neorecormon EPO for post-haemorrhagic anaemia; **g,h,** urine from two cyclists from Tour de France 1998 (samples concentrated by ultrafiltration). Note the 'mixed' appearance of the pattern in **e**. The cathode is at the top; pH values are indicated on the left.

We assayed 102 frozen urine samples from participants in the Tour de France 1998 cycling competition for EPO by using an enzyme-linked immunosorbent assay. Twenty-eight of these samples had EPO levels above the normal range of 0–3.7 international units per litre (mean, 0.48 IU per litre, $n = 103$; 77 samples were below the minimum detectable concentration of 0.6 IU per litre). We analysed the 14 samples presenting with the highest concentrations (7–20 IU per litre): although characterization of the EPO source does not require such high levels for urine analysis, we selected these samples for isoelectric focusing as they were more likely to contain exogenous hormone; indeed, they all gave rise to a banding pattern typical of recombinant hormone.

Our method for detecting recent exposure to recombinant EPO in athletes could be useful for in-competition controls in events of long duration (for example, cyclists have been known to use exogenous EPO continuously for 6 months at a time), but should find its principal application in out-of-competition testing.

Françoise Lasne, Jacques de Ceaurriz
National Anti-Doping Laboratory, 92290 Châtenay-Malabry, France

1. Casoni, I. *et al. Int. J. Sports Med.* **14,** 307–311 (1993).
2. Gareau, R. *et al. Nature* **380,** 113 (1996).
3. Wide, L. *et al. Med. Sci. Sports Exerc.* **27,** 1569–1576 (1995).
4. Rademacher, T. W., Parekh, R. B. & Dwek, R. A. *Annu. Rev. Biochem.* **57,** 785–838 (1988).

Phylogeny

Parabasalian flagellates are ancient eukaryotes

Discrepancies between eukaryotic phylogenetic trees based on different gene sequences have led to the suggestion that the deepest branches of each gene tree could simply be artefacts of rapid evolution rather than indicators of an ancient divergence[1–5]. But if an insertion or deletion occurred in a gene sequence very early in eukaryotic evolution, the oldest eukaryotic lineages should be recognizable by their resemblance to prokaryotes lacking this character. Here we investigate the structure of the gene encoding enolase, an enzyme of the glycolytic pathway, and find that the gene from parabasalian flagellates lacks two deletions present in other eukaryotic enolases, indicating that Parabasalia could be the most ancient eukaryotes examined so far.

Eukaryotic enolase sequences contain several insertions and deletions compared with each other, Eubacteria and Archaebacteria, some of which have been used to link animals and fungi[6]. We sequenced enolase genes from three putatively ancient lineages: diplomonads, Parabasalia and kinetoplastids. Neither kinetoplastid nor diplomonad enolase genes are exceptional (nor is that of *Entamoeba* enolase, another putatively ancient eukaryote), but parabasalian enolases lack two close, single-amino-acid deletions common to all other eukaryotic enolases (Fig. 1a, overleaf).

Given the proximity of these deletions, they may have resulted from a single event. However, the surrounding alignment is reproducible, and the amino acids at these

positions are identical or similar in Parabasalia and prokaryotes. The simplest explanation is that parabasalian enolases have retained the ancestral, prokaryotic state while the common ancestor of other eukaryotic enolases sustained two deletions. This is consistent with enolase phylogeny (Fig. 1b), although the position of parabasalian enolases must be treated with the extreme caution demanded by deep branches[1–5], particularly as parabasalian enolases are quite divergent. The phylogeny is important, however, because it shows that these deletions in the enolase gene do not simply reflect a lateral transfer of enolase from a prokaryote to Parabasalia.

Other explanations for these observations cannot be excluded, such as parallel deletions in two or more lineages of non-parabasalian eukaryotes, deletions in the common ancestor of all eukaryotes and subsequent re-insertion of these two amino acids in Parabasalia, or recombination with a prokaryotic enolase. However, these are all more complex, and the consistency between enolase deletions and molecular phylogeny, and the lack of opposing evidence, favours the explanation that Parabasalia are the earliest extant lineage of eukaryotes studied.

Clues to the nature of the ancestral eukaryote might be gleaned by comparing Parabasalia with other eukaryotes. One difference is that Parabasalia lack mitochondria, containing instead an anaerobic metabolic organelle called a 'hydrogenosome'[7]. The parabasalian hydrogenosome is derived from the mitochondrial lineage[7,8], and hydrogenosomes have evolved from mitochondria in several other lineages[8]. Parabasalian hydrogenosomes may also have evolved from a fully specialized mitochondrion, but, if Parabasalia are extremely ancient, their hydrogenosomes might have evolved from an unspecialized proto-mitochondrial symbiont that developed its bioenergetic capacity by a different route from typical mitochondria[7,9].

A better understanding of this and other atypical features of Parabasalia (for example, mitosis, meiosis and transcription initiation[10]) may reveal whether such characters reflect the primitive state of eukaryotes or odd derivations in Parabasalia. Conversely, the ordinary aspects of Parabasalia (they too have a nucleus, cytoskeleton, flagella, Golgi bodies and spliceosomes[11]) indicate that many important characteristics were established in the ancestor of extant eukaryotes. Parabasalia, then, are not major intermediates in a gradual transition between prokaryote and eukaryote and, should such an intermediate lineage still exist, it is unlikely to have been characterized.

Discovering primitive molecular characteristics is perhaps our best hope of identifying ancient eukaryotic lineages, although

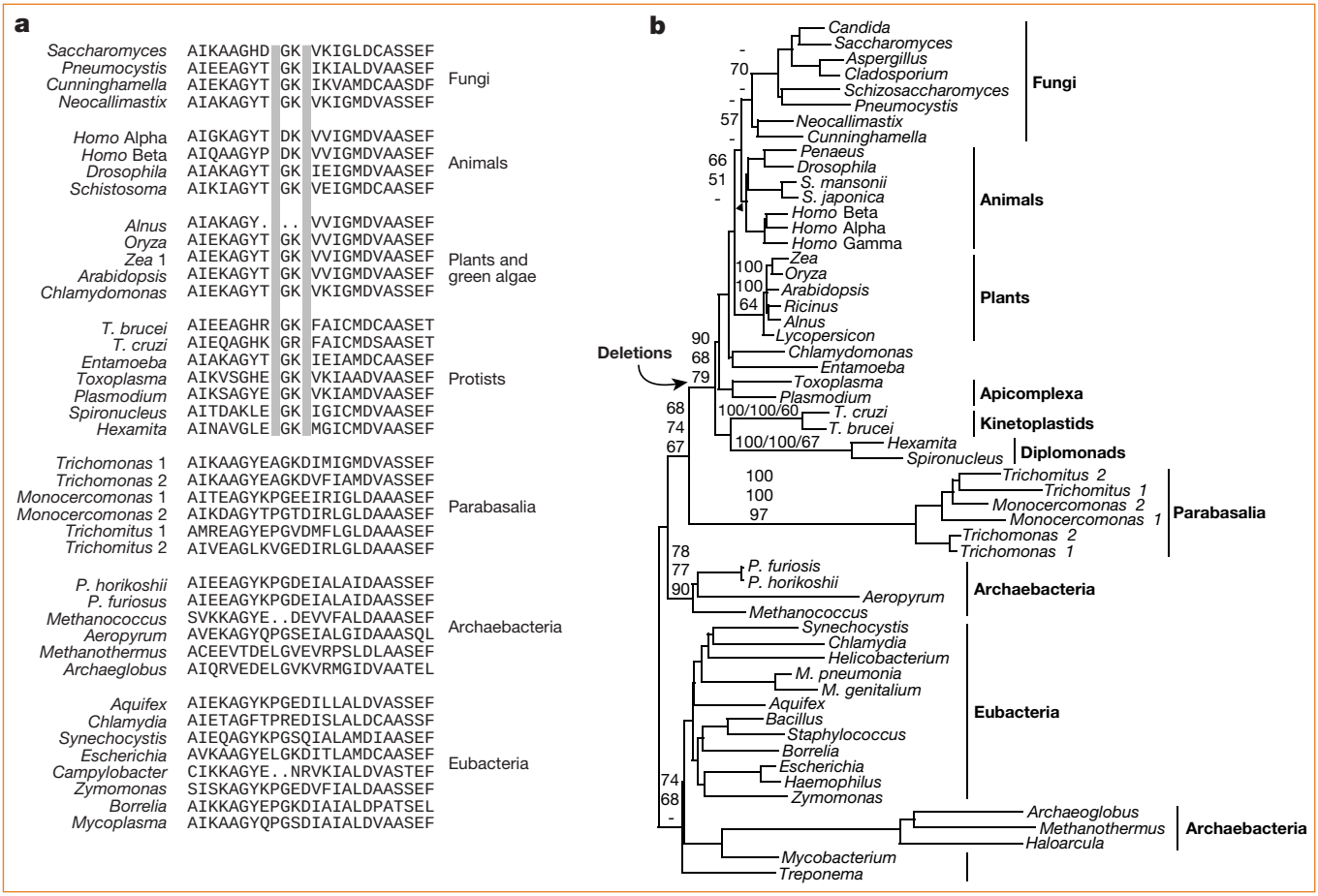

Figure 1 Evidence from enolase structure that Parabasalia are the most ancient eukaryotes. **a,** Deletions in enolase found in all eukaryotes except Parabasalia (shaded). Independent deletions also occurred in *Alnus, Methanococcus* and *Campylobacter* (not shaded). Positions shown correspond to amino acids 232–253 of the *Saccharomyces* gene. **b,** Phylogeny of enolase. Numbers at nodes are bootstrap values without gamma correction (top), bootstrap values with gamma correction (middle), and per cent occurrence in 10,000 quartet puzzling trees (bottom). Only values over 50% for major nodes are shown. Enolase genes were amplified from *Spironucleus vourtens* (ATCC 50386), *Hexamita inflata* (AZ-4), *Trypanosoma cruzi* (Cl-Brenner), *T. brucei* (lsTat 1.1a), *Trichomonas vaginalis* (NIH-C1, ATCC 30001), *Trichomitus batrachorum* (G11), and *Monocercomonas* sp. (Ns-1PRR, ATCC 50210). DNA was provided by M. Müller, H. van Keulen and J. Feagan. Polymerase chain reaction products were cloned using TOPO TA vector (Invitrogen) and multiple clones from each species were sequenced on both strands. GenBank accession numbers for new sequences are AF159517–AF159532. Inferred amino-acid sequences were aligned with known homologues using PIMA and edited manually. The region shown in **a** was realigned by different investigators using several algorithms and models, consistently giving the alignment shown. Trees were inferred from 372 amino acids deemed to be homologous among all three domains. Distances and bootstrap distances (using Puzzleboot, by M. Holder and A. Roger) were calculated with PUZZLE 4.0.1 using the JTT substitution matrix and amino-acid frequency estimated from the data. Site-to-site rate variation was modelled on a gamma distribution with eight rate categories plus invariant sites and the shape parameter was estimated from the data. Trees were constructed using BioNJ (other methods also gave the same placement of Parabasalia). Maximum-likelihood trees were inferred using quartet/9 puzzling with 10,000 puzzling steps and the PUZZLE settings described above.

sadly our sampling from those protists most likely to contain these is limited. Other characteristics distinguishing Parabasalia as the earliest eukaryotic lineage are waiting to be discovered — confirmation of the ancient origin of Parabasalia may depend on these characteristics being common in parabasalian genomes.

Patrick J. Keeling*†, Jeffrey D. Palmer*

**Department of Biology, Indiana University, Bloomington, Indiana 47405, USA*

†Present address: Canadian Institute for Advanced Research, Department of Botany, University of British Columbia, Vancouver, British Columbia V6T 1Z4, Canada

e-mail: pkeeling@interchange.ubc.ca

1. Embley, T. M. & Hirt, R. P. *Curr. Opin. Genet. Dev.* **8,** 624–629 (1998).
2. Philippe, H. & Laurent, J. *Curr. Opin. Genet. Dev.* **8,** 616–623 (1998).
3. Keeling, P. J. *BioEssays* **20,** 87–95 (1998).
4. Stiller, J. W. & Hall, B. D. *Mol. Biol. Evol.* **16,** 1270–1279 (1999).
5. Roger, A. J. *et al. Mol. Biol. Evol.* **16,** 218–233 (1999).
6. Baldauf, S. L. & Palmer, J. D. *Proc. Natl Acad. Sci. USA* **90,** 11558–11562 (1993).
7. Müller, M. *Parasitol. Today* **13,** 166–167 (1997).
8. Embley, T. M., Horner, D. A. & Hirt, R. P. *Trends Ecol. Evol.* **12,** 437–441 (1997).
9. Martin, W. & Müller, M. *Nature* **392,** 37–41 (1998).
10. Liston, D. R. & Johnson, P. J. *Mol. Cell. Biol.* **19,** 2380–2388 (1999).
11. Fast, N. M. & Doolittle, W. F. *Mol. Biochem. Parasitol.* **99,** 275–278 (1999).

Planetary science

Tectonics and water on Europa

The tectonics of Europa, one of Jupiter's moons, are complex. This satellite probably hosts a subsurface water ocean, but the thickness of the outer ice crust is poorly constrained and the episodic presence of liquid water at the surface is debated. We argue that some surface features of Europa are formed by soft ice that is heated by viscous dissipation of tidal motion along faults, and do not depend on a shallow ocean. Our model suggests that transient pockets of liquid water or brine could form at shallow depths in the crust.

The Galileo spacecraft has returned high-resolution images of surface lineations and ridges on Europa. These have prompted proposals that tidal stresses from Jupiter may fracture the icy crust of the synchronously rotating satellite, allowing material from the interior to reach the surface[1,2]. One model invokes tidal expansion and contraction of metre-wide cracks which repeatedly force liquid water up from a subsurface ocean to the surface of the moon as it completes each 85-hour orbit[3] — a process that depends on a thin (1 km or less) ice shell and which has fuelled speculation that the ocean frequently meets the sunlit surface and could be a habitat for life.

The formation of kilometre-deep cracks in Europa's crust is a problem. Below a depth of 35 m, the pressure from the weight of the overlying ice will exceed the estimated stresses due to tides ($<4\times10^4$ Pa) and prevent cracks from growing. Any fractures will halt at a depth where warmer, less viscous ice flows, rather than fracturing further, to accommodate tidal strain. Taking an estimated strain rate of 2×10^{-10} s^{-1} and a relation between normal stress and yield stress appropriate for ice[4], we find that the brittle–ductile transition occurs at depths where temperatures[5] exceed 170 K, well above those of any ice–ocean interface.

Also, liquid water in a crack will freeze solid by virtue of the conduction of heat to the walls: the freezing time is $t=w^2/(16\kappa\lambda^2)$, where w is the crack width, κ is the thermal diffusivity of ice (1.7×10^{-6} m^2 s^{-1}) and λ is a dimensionless parameter[6] equal to about 0.3. A 1-m crack will freeze in 1.3 orbits. Hydrostatic forces are too weak to extrude ice from such a narrow orifice and, unless a compensatory removal of crust occurs elsewhere, the crack will disappear.

We propose, alternatively, that tides drive viscous flow and heating by dissipation at zones of lateral motion (strike–slip) in the crust. There is accumulating evidence for strike–slip motion on Europa[7]. The relative motion along a fault or defect will produce frictional heating, causing the local temperature to increase and the viscosity of the ice to decrease[8]. This feedback can lead to accommodation of the relative motion of two blocks of crust by viscous flow in a zone of finite width, rather than a discontinuity at a fault. Steady-state conditions in the zone are derived by equating the production of heat by viscous dissipation with its loss by conduction to the surrounding ice.

Strike–slip motion of amplitude a at a diurnal period t (3×10^5 s) will maintain a temperature T_c and viscosity η_c at the centre of the shear zone[6] that satisfy $16kRT_c^2t^2=\pi^2\eta_cE_aa^2$, where E_a and k are the activation energy (6×10^4 J at 273 K) and thermal conductivity (2.1 W m^{-1} K^{-1} at 273 K), respectively, of the ice, and R is the gas constant.

A plausible diurnal motion[3] of 0.6 m can maintain the ice in the centre of the shear zone at a temperature of 273 K, where its viscosity will be roughly 10^{13} Pa s. The width of this zone of soft ice is $\delta=\eta a(\tau t)^{-1}$, where τ is the shear stress (about 1 km for $\tau=2\times10^4$ Pa). This warm ice will have a buoyant density contrast $\Delta\rho=20$ kg m^{-3} with respect to the surrounding ice and will flow upwards by a few tens of centimetres over the course of one tidal cycle.

We suggest that such motion over the course of many cycles could be responsible for the formation of structures such as ridge pairs. Our model does require the existence of an ocean (not necessarily shallow): without the mechanical decoupling between the ice crust and the interior, the motion of the crust would be 30–50 times smaller.

Larger strike–slip motion may lead to partial melting (liquid water) in the shear zone. The melt-generation rate scales as $\tau^2(\rho\eta_cL)^{-1}$, where L and ρ are the latent heat of fusion (3.25×10^5 J kg^{-1}) and density (900 kg m^{-3}), respectively, of ice. This production will be balanced by downward percolation of the denser melt at a rate[9] $A\phi^n\Delta\rho g(\eta_mh)^{-1}$, where A and n are constants, ϕ is the melt fraction, η_m is the melt viscosity, h is the thickness of the melt column, and g (1.3 m s^{-2}) is Europa's surface gravity. Although there are considerable uncertainties in some of these values, the equilibrium melt fraction is of the order of 1%. This much melt will form only if the strike–slip motion is sufficiently large ($\sim$1 m) to compensate for the reduction in ice viscosity by a factor of about one third as a result of the presence of melt[10].

The pore pressure due to the presence of melt will also increase the depth to the brittle–ductile transition and allow fractures to accommodate strike–slip motion and to slow heat generation. Melt pockets below the fracture zone will percolate downwards at a velocity of a few tens of metres per year, and so will have a lifetime of $\sim$1,000 years. Any melt at the base of the fracture zone will escape through the fractures or freeze and, if salts are present, brines will be rejected from the freezing melt[11].

In this case, the melt lifetime, estimated by equating the latent heat that must be rejected to the rate of thermal conduction away from the fault zone, will be about 30 years (although shorter at shallow depths, where vertical conduction to the surface is important). Depending on the thickness of the fractured zone, transient liquid-water or brine pockets may exist within reach of sunlight, potentially providing habitats for photosynthetic organisms capable of remaining dormant in ice for millennia[12] between relatively brief 'blooms'.

Eric J. Gaidos*, Francis Nimmo†

**Jet Propulsion Laboratory, California Institute of Technology, 4800 Oak Grove Drive, Pasadena, California 91109, USA*

†Bullard Laboratories, Department of Earth Sciences, Madingley Rise, Madingley Road, University of Cambridge, Cambridge CB3 0EZ, UK

1. Sullivan, R. *et al. Nature* **391,** 371–373 (1998).
2. Pappalardo, R. T. *et al. J. Geophys. Res.* **104,** 24015–24055 (1999).
3. Greenberg, R. *et al. Icarus* **135,** 64–78 (1998).
4. Rist, M. A. *J. Phys. Chem. B* **101,** 6263–6266 (1997).
5. Pappalardo, R. T. *et al. Nature* **391,** 365–367 (1998).
6. Turcotte, D. L. & Schubert, G. *Geodynamics: Applications of Continuum Physics to Geological Problems* (Wiley, New York, 1982).
7. Tufts, B. R. *et al. Icarus* **141,** 53–64 (1999).
8. Stevenson, D. J. in *Europa Ocean Conf., Capistrano Conf.* 5 69–70 (San Juan Capistrano Res. Inst., CA, 1996).
9. McKenzie, D. *Earth Planet. Sci. Lett.* **74,** 81–91 (1985).
10. Duval, P. *Int. Assoc. Sci. Hydro.* **118,** 29–33 (1977).
11. Cottier, F., Eiken, H. & Wadhams, P. *J. Geophys. Res.* **104,** 15850–15871 (1999).
12. Vorobyova, E. *et al. FEMS Microbiol. Rev.* **20,** 277–290 (1997).